Systems/Circuits

α_{2A}-Adrenergic Receptors Filter Parabrachial Inputs to the Bed Nucleus of the Stria Terminalis

Stephanie A. Flavin,[1,3] Robert T. Matthews,[1,2,3] Qin Wang,[5] E. Chris Muly,[4] and Danny G. Winder[1,2,3]

[1]Department of Molecular Physiology & Biophysics, [2]John F. Kennedy Center for Research on Human Development, and [3]Neuroscience Program in Substance Abuse, Vanderbilt Brain Institute, Vanderbilt University School of Medicine, Nashville, Tennessee 37232-0615, [4]Department of Psychiatry, Emory University School of Medicine, Atlanta, Georgia 30322, [5]Department of Cell, Developmental and Integrative Biology, University of Alabama at Birmingham, Birmingham, Alabama 35294

α_2-adrenergic receptors (AR) within the bed nucleus of the stria terminalis (BNST) reduce stress–reward interactions in rodent models. In addition to their roles as autoreceptors, BNST α_{2A}-ARs suppress glutamatergic transmission. One prominent glutamatergic input to the BNST originates from the parabrachial nucleus (PBN) and consists of asymmetric axosomatic synapses containing calcitonin gene-related peptide (CGRP) and vGluT2. Here we provide immunoelectron microscopic data showing that many asymmetric axosomatic synapses in the BNST contain α_{2A}-ARs. Further, we examined optically evoked glutamate release *ex vivo* in BNST from mice with virally delivered channelrhodopsin2 (ChR2) expression in PBN. In BNST from these animals, ChR2 partially colocalized with CGRP, and activation generated EPSCs in dorsal anterolateral BNST neurons that elicited two cell-type-specific outcomes: (1) feedforward inhibition or (2) an EPSP that elicited firing. We found that the α_{2A}-AR agonist guanfacine selectively inhibited this PBN input to the BNST, preferentially reducing the excitatory response in *ex vivo* mouse brain slices. To begin to assess the overall impact of α_{2A}-AR control of this PBN input on BNST excitatory transmission, we used a Thy1-COP4 mouse line with little postsynaptic ChR2 expression nor colocalization of ChR2 with CGRP in the BNST. In slices from these mice, we found that guanfacine enhanced, rather than suppressed, optogenetically initiated excitatory drive in BNST. Thus, our study reveals distinct actions of PBN afferents within the BNST and suggests that α_{2A}-AR agonists may filter excitatory transmission in the BNST by inhibiting a component of the PBN input while enhancing the actions of other inputs.

Key words: **adrenergic receptors; bed nucleus of the stria terminalis; excitatory transmission; extended amygdala; norephinephrine; optogenetics**

Introduction

Risk of relapse to drug-seeking behavior in addicts remains high even after treatment (Weiss and Koob, 2001), and stress increases relapse risk (Brown et al., 1995; Sinha et al., 1999; Sinha et al., 2011). In recent studies, α_2-AR agonists have shown promise in curbing cravings in drug-addicted individuals (Sinha et al., 2007; Jobes et al., 2011; Fox and Sinha, 2014; Fox et al., 2014). These clinical data are supported by rodent data demonstrating that α_2-AR agonists reduce stress-induced reinstatement of drug-seeking behavior in rats (Erb et al., 2000; Shaham et al., 2000; Highfield et al., 2001; Mantsch et al., 2010).

Noradrenergic signaling in the bed nucleus of the stria terminalis (BNST) plays an important role in stress-induced relapse to drug-seeking behavior (Aston-Jones et al., 1999; Erb et al., 2001; Flavin and Winder, 2013). Direct administration of α_2-AR agonists into the BNST reduces stress-induced reinstatement of drug-seeking behavior (Wang et al., 2001), as well as conditioned place aversion from morphine withdrawal (Delfs et al., 2000). α_{2A}-ARs are widely expressed in the BNST (Shields et al., 2009). In addition to their autoreceptor function, α_{2A}-ARs in the BNST can heterosynaptically modulate excitatory transmission (Shields et al., 2009; Krawczyk et al., 2011). The BNST receives many glutamatergic inputs from which α_{2A}-ARs may modulate excitatory transmission. A better understanding of which excitatory inputs to the BNST are selectively modulated by α_{2A}-ARs may help elucidate neural circuitry underlying the ability of α_2-AR agonists to block stress-induced reinstatement of drug-seeking in rodent models.

One of the more prominent glutamatergic inputs to the BNST is an ascending input from the parabrachial nucleus (PBN) (Shimada et al., 1985; Shimada et al., 1989; Dobolyi et al., 2005) that forms axosomatic synapses onto dorsal BNST neurons (Shimada et al., 1989; Dobolyi et al., 2005). These axosomatic inputs contain both the neuropeptide calcitonin gene-related peptide (CGRP) as well as vGluT2 (Shimada et al., 1985; Shimada et al.,

Received Feb. 24, 2014; revised June 2, 2014; accepted June 6, 2014.

Author contributions: S.A.F., R.T.M., Q.W., E.C.M., and D.G.W. designed research; S.A.F., R.T.M., and E.C.M. performed research; S.A.F., R.T.M., and E.C.M. analyzed data; S.A.F., R.T.M., E.C.M., and D.G.W. wrote the paper.

This work was supported by National Institutes of Health Grants DA019113, F30DA034428, and RR000165. Imaging and image data analyses were performed in part through the use of the Vanderbilt University School of Medicine Cell Imaging Shared Resource (supported by National Institutes of Health Grants CA68485, DK20593, DK58404, DK59637, and EY08126). We thank Dr. Ron Emeson for providing the CGRP knock-out mouse line.

The authors declare no competing financial interests.

Correspondence should be addressed to Dr. Danny G. Winder, Department of Molecular Physiology & Biophysics, 23rd and Pierce Avenue S, Room 754, RRB, Vanderbilt University School of Medicine, Nashville, TN 37232-0615. E-mail: danny.winder@vanderbilt.edu.

DOI:10.1523/JNEUROSCI.0822-14.2014

Copyright © 2014 the authors 0270-6474/14/349319-13$15.00/0

1989; Dobolyi et al., 2005; Niu et al., 2010; Kaur et al., 2013). The PBN input to the extended amygdala, which includes both the BNST and the central nucleus of the amygdala (CeA), has been implicated in a wide range of behaviors, including pain sensitization (Han et al., 2005, 2010), taste aversion (Mungarndee et al., 2006), fear conditioning (Sink et al., 2013a), hypercapnic arousal (Kaur et al., 2013), and feeding (Carter et al., 2013). Previous studies using electrical stimulation to target glutamatergic inputs suggest that α_2-ARs may differentially modulate the PBN and basolateral amygdala (BLA) inputs to the CeA (Delaney et al., 2007).

Here we demonstrate that the α_{2A}-AR agonist guanfacine selectively regulates a PBN input to the BNST. We also show that optical PBN afferent stimulation in the BNST generates two different responses and that these responses are differentially inhibited by guanfacine. Conversely, we show that, in a mouse line where ChR2 is widely expressed but not colocalized with BNST CGRP, α_{2A}-AR activation enhances the response to other inputs, suggesting a role in filtering information.

Materials and Methods

Microinjection surgeries. Five- to 10-week-old male C57BL/6J mice (The Jackson Laboratory) were used. All mice were group-housed and on a 12 h light/dark cycle. Mice were given access to food and water *ad libitum*. During surgeries, mice were anesthetized with isoflurane and injected intracranially with an adeno-associated virus (AAV5) encoding channelrhodopsin (ChR2) fused to YFP, under the control of a CaMKIIα promoter (AAV-CaMKIIα-ChR2:YFP; University of North Carolina Vector Core). A targeted microinjection of the virus (100–150 nl) was made into one of the following sites according to the Paxinos and Franklin (2004) mouse brain atlas: the BLA (anteroposterior, −1.58; mediolateral, ±2.90; dorsoventral, −5.11) or the PBN (anteroposterior, −5.34; mediolateral, ±1.26; dorsoventral, −3.64). Mice were treated with 1 mg/kg injections of ketoprofen for 72 h after surgery. Virally injected mice were killed 6–12 weeks after surgery for anatomical and electrophysiological analysis.

To confirm specificity of injection into the PBN, 7 male C57BL/6J mice (The Jackson Laboratory) 7–10 weeks old were injected with 150 μl of AAV5-CaMKIIα-ChR2:YFP virus unilaterally into the hindbrain, targeted to the PBN. After 6 weeks' survival, brains were removed under deep Nembutal anesthesia and immersion fixed in 4% PFA. Frozen sections were cut on a cryostat, and the locations of injection sites were compared with fiber densities in the ipsilateral BNST by imaging for ChR2-YFP fluorescence. Few or no fibers were seen in the BNST when injection sites were lateral, rostral, or caudal to the PBN ($n = 1$ each). Injections medial to the PBN were avoided because of the known projections of the locus ceruleus to the BNST (Aston-Jones et al., 1999). In two mice, virus injections appeared to be confined to the dorsal PBN, and only a few ChR2-YFP-positive fibers were visible in each 40 μm section of the BNST. In two other mice, the injection site included both dorsal and ventral parts of the PBN and a moderate density of ChR2-YFP fibers was seen in the BNST (see Fig. 1*D1*). Henceforth, viral injections were targeted to both dorsal and ventral PBN. When the viral injection site was confined to the PBN, ChR2-YFP fibers in the BNST were tyrosine hydroxylase-negative ($n = 2$), suggesting that afferents from the locus ceruleus were not part of the ChR2-YFP-positive fiber population imaged and light activated in this study (data not shown).

Fluorescent immunohistochemistry. For immunohistochemical colocalization studies, 6 additional male C57BL/6J mice that had the AAV5-CaMKIIα-ChR2:YFP virus injected into the PBN 6 weeks earlier, and three B6.Cg-Tg(Thy1-COP4/EYFP)9Gfng (Thy1-COP4) transgenic mice (The Jackson Laboratory, strain ID 007615), were transcardially perfused with 10 ml of ice-cold PBS, followed by 20 ml of ice-cold 4% PFA in PBS. Thy1-COP4 transgenic mice express ChR2-YFP widely in the brain under the direction of the pan-neuronal Thy1 promoter. Multiple founder lines exist with variations in overall expression pattern, likely because of differences in copy number and insertion site of the transgene (Arenkiel et al., 2007). Brains were postfixed in 4% PFA overnight at 4°C and were then transferred into 30% sucrose and stored for 2–10 d at 4°C. Coronal sections were cut on a cryostat (Leica, CM3050S) at a thickness of 40 μM. Sections containing the BNST were free-floated in PBS for immunolabeling. Sections were permeabilized for 30 min with 0.5% Triton X-100 in PBS at room temperature (RT). Next, nonspecific binding was blocked with 10% normal donkey serum in PBS containing 0.1% Triton X-100 for 1 h at RT. Sections were then incubated in primary antibody in PBS containing 0.1% Triton X-100 for 2 d at 4°C, followed by 4 × 10 min PBS washes. Sections were then incubated overnight at 4°C with secondary antibodies in PBS containing 0.1% Triton X-100. Finally, sections were washed with PBS (4 × 10 min), mounted on Fisher + slides (Fisher Scientific), and coverslipped with PolyAquamount (Polysciences).

Images of fluorescent marker-labeled brain sections and viral vector injection sites were taken with a Zeiss 710 confocal microscope. Lenses used included a 20×/0.80 NA Plan-Apochromat and a 63×/1.4 NA Plan Apochromat oil. Excitation/emission wavelengths (nm) for each fluorophor were as follows: Dylight 405, 405/410–505; YFP, 512/519–553; cy3, 561/566–600; cy5, 633/638–759. Mosaic image stitching was done with Zeiss ZEN software.

Image analysis. The neuropeptide CGRP is a marker of the PBN input to the BNST (Shimada et al., 1985, 1989; Dobolyi et al., 2005). We sought to further illustrate the level of colocalization of CGRP immunofluorescence with ChR2-YFP fluorescence in the BNST of both Thy1-COP4 mice and mice that had PBN injections of AAV5-CaMKIIα-ChR2:YFP. We did this as a means of assessing the relative expression of ChR2 on PBN terminals in the BNST of these two types of mice. We used ImageJ (Fiji) software to visualize the colocalization of CGRP immunohistochemistry fluorescence with ChR2-YFP fluorescence in the BNST. From each of these types of mice, we selected images (63×) of BNST cells that had an observed CGRP-containing axosomatic contact, as CGRP-containing axosomatic synapses are found in projections from the PBN to the dorsal BNST (Dobolyi et al., 2005). We then drew a line through the selected cell body as well as the neuropil immediately surrounding the soma. We next individually plotted the gray value (y-axis) versus distance (μm) for each of the different fluorescent markers (CGRP, ChR2, or NeuN) along the line that we drew through the soma and the immediately surrounding neuropil. Next, we overlaid each of the fluorescent profiles using PRISM software to visualize the level of overlap in the localization of CGRP, ChR2-YFP, or NeuN.

Electron microscopy. For immunoelectron microscopy, mice were killed and perfused with 4% PFA, 0.2% glutaraldehyde, and 0.2% picric acid in PBS. We perfused hemagglutinin (HA) α_{2A}-AR knock-in (HA α_{2A}-AR KI) mice that label the N terminus of the α_{2A}-AR with an HA tag. This mouse line was developed by Q.W. The HA-tag on the α_{2A}-AR allows us to use HA antibodies to more easily visualize α_{2A}-AR expression, as α_{2A}-AR antibodies show poor specificity.

In some cases, the mice were pretreated with the α_2-AR agonist clonidine to induce internalization of the HA-tagged α_{2A}-AR. Animals were given intraperitoneal clonidine (1 mg/kg) 30 min before death. The brains were blocked and postfixed in 4% PFA for 4 h. Coronal, 50-μm-thick vibratome sections of the brain were cut and stored frozen at −80°C in 15% sucrose until immunohistochemical experiments were performed. The care of the animals and all anesthesia and sacrifice procedures in this study were performed according to the National Institutes for Health Guide for the Care and Use of Laboratory Animals and were approved by the Institutional Animal Care and Use Committee of Emory University.

Single-label immunoperoxidase labeling was performed using a mouse monoclonal antibody against the HA tag at a 1:500 dilution (Covance, clone 16B12). The single-label immunoperoxidase labeling was performed as described previously (Muly et al., 2003). Briefly, sections were thawed, incubated in blocking serum (3% normal goat serum, 1% BSA, 0.1% glycine, 0.1% lysine in 0.01 M PBS, pH 7.4) for 1 h and then placed in primary antiserum diluted in blocking serum. After 36 h at 4°C, the sections were rinsed and placed in a 1:200 dilution of biotinylated horse anti-mouse IgG (Vector) for 1 h at RT. The sections were then rinsed, placed in avidin-biotinylated peroxidase complex (ABC Elite,

Vector) for 1 h at RT, and then processed to reveal peroxidase using DAB as the chromagen. Sections were then postfixed in osmium tetroxide, stained *en bloc* with uranyl acetate, dehydrated, and embedded in Durcupan resin (Electron Microscopy Sciences). Selected regions of the BNST were mounted on blocks, and ultrathin sections were collected onto pioloform-coated slot grids and counterstained with lead citrate. Control sections processed as above, except for the omission of the primary immunoreagent, did not contain DAB label upon electron microscopic examination.

Ultrathin sections were examined with a Zeiss EM10C electron microscope and immunoreactive elements were imaged using a Dualvision cooled CCD camera (1300 × 1030 pixels) and Digital Micrograph software (version 3.7.4, Gatan). Images selected for publication were saved in TIFF format and imported into an image processing program (Canvas 8; Deneba Software). The contrast was adjusted, and the images were cropped to meet size requirements.

In considering the results of our immunoelectron microscopic examination of α_{2A}-AR, there are several caveats. First, it is possible that the presence of the HA tag on the knock-in transgenic mouse resulted in an alteration in the subcellular distribution of the receptor. However, other studies of α_{2A}-AR receptor localization have found it is localized in dendritic, axonal, and glial compartments in the locus ceruleus (Lee et al., 1998), the ventrolateral medulla (Milner et al., 1999), and hippocampus (Milner et al., 1998), so if the presence of the HA tag had an effect on localization, it appears to have been of a quantitative nature, and not such as to qualitatively change the localization pattern. A second issue was our use of clonidine pretreatment. We found this necessary because the HA tag is located on an extracellular portion of the receptor and in untreated animals the majority of the label appeared to be extracellular, outlining adjacent structures. It is possible that the clonidine-induced internalization also induced transport from axon terminals and dendritic spines to more proximal positions in the dendritic and axonal arbors. In clonidine-treated animals, we observed that dendritic shafts and preterminal axons were the most commonly labeled structures; however, it is possible that spines and axon terminals would have been more common without clonidine treatment.

Electrophysiology recordings in the BNST: brain slice preparation. Brain slice preparation methods were used as previously described (Grueter and Winder, 2005; Grueter et al., 2006; Shields et al., 2009). Mice were removed from colony and allowed to acclimate for 1 h in a Med Associates sound-attenuating chamber. After the acclimation, mice were anesthetized with isofluorane and then decapitated. Brains were removed quickly and transferred to a 1°C–4°C oxygenated, low sodium sucrose dissecting solution (in mM: 194 sucrose, 20 NaCl, 4.4 KCl, 2 $CaCl_2$, $MgCl_2$, 1.2 NaH_2PO_4, 10 glucose, 26 $NaHCO_3$). A Leica vibratome was used to prepare coronal brain slices (300 μm) containing the dorsal BNST. Slices were then transferred to either an interface chamber for field potential recordings or to a holding chamber for whole-cell recordings. Both the interface chamber and the holding chamber contained heated, oxygenated ACSF that was composed of (in mM) as follows: 124 NaCl, 4.4 KCl, 2.5 $CaCl_2$, 1.3 $MgSO_4$, 1 NaH_2PO_4, 10 glucose, and 26 $NaHCO_3$.

Field potential recordings. For field potential recordings, Thy1-COP4 transgenic mice of at least 5 weeks in age were used. Slice preparation for field potential recordings in the dlBNST was performed as previously reported (McElligott and Winder, 2008). Picrotoxin (25 μM) was added to all recordings to isolate excitatory transmission. For optical field potential recordings, light stimulation was produced from a Lamba XL light source (Sutter Instruments) and shone through a bandpass filter (Semrock, 475 nm wavelength, 20 nm bandwidth). The blue light was guided from the light source through a water-shielded cable that was positioned ~5 cm above the surface of the slice, resulting in full-field illumination. The light stimulation produced a shift in potential, the optical field potential (oN) that was shown to be NBQX-sensitive (decreased 76% from mean, $n = 2$), similar to the N2 seen in electrical field potential recordings previously described (Weitlauf et al., 2004; Egli et al., 2005; Grueter and Winder, 2005). pClamp software (Molecular Devices) controlled light pulse duration and frequency. For optical field potential recordings, light stimuli were ~2 ms in duration and occurred every 20 s. All field potential data were collected using Clampex 10.2 (Molecular Devices).

Analysis of field potential recordings. All field potential recordings were analyzed via Clampfit 10.2 (Molecular Devices) as previously described (Shields et al., 2009). All field recordings contain a 20 min baseline before agonist application, with the exception of the atipamezole preincubated experiments for which atipamezole was present during baseline, and all data points are normalized to the baseline 5 min before agonist application. Plotted time courses for field experiments are represented as 1 min averages.

Optical whole-cell recordings. Whole-cell voltage-clamp recordings were performed as previously reported (Grueter and Winder, 2005; Grueter et al., 2006; Kash and Winder, 2006; Silberman et al., 2013). Briefly, after brain slice preparation, slices recovered for 1 h in a submerged holding chamber (25°C) containing oxygenated (95% O_2/5% CO_2) ACSF. After recovery in the holding chamber, slices were transferred to the recording chamber where they were continuously perfused with oxygenated and heated (25°C) ACSF at a rate of 2 ml/min. For optical whole-cell recordings, light stimulation was produced from a Lamba XL light source (Sutter Instruments) shone through a bandpass filter (Semrock, 475 nm wavelength, 20 nm bandwidth). The blue light was guided from the light source through the objective lens using a double lamp-housing adapter (Olympus), resulting in illumination of the slice. Light stimuli were ~2 ms in duration and occurred every 10–20 s. oEPSCs of 100–1000 pA were recorded while voltage-clamped at −70 mV in the presence of picrotoxin (25 μM). Although we did not quantify the levels of viral expression for comparison between the BLA and the PBN, we adjusted initial oEPSCs from each of the inputs such that all baseline oEPSCs were between 100 and 650 pA at the beginning of each experiment. For large starting oEPSCs, neutral density filters and microscope apertures were used to adjust light intensity such that all experiments were recorded on baseline oEPSCs within the defined amplitude range. Evoked oEPSCs were of a short, invariant latency, consistent with monosynaptic excitation. In data analysis, oEPSCs were normalized to the amplitude of the baseline oEPSCs recorded. After achieving whole-cell configuration, cells were allowed to equilibrate for a minimum of 5 min before baseline was started. Postsynaptic parameters were monitored continuously throughout the duration of the experiments. Data are represented as an average of the peak amplitude of 3 sweeps. For voltage-clamp recordings, electrodes of 2.5–5.0 MΩ were filled with (in mM) as follows: 117 Cs gluconate, 20 HEPES, 0.4 EGTA, 5 TEA, 2 MgCl, 4 Na_2ATP, 0.3 NA_2GTP (pH 7.2–7.4, osmolarity 290–295). Input resistance, holding current, and series resistance are monitored continuously. Experiments with input resistances that change by ≥20% are excluded from data analysis. All whole-cell data were recorded with Clampex version 10.2 and analyzed with pClamp version 10.2 (Molecular Devices).

Whole-cell optical current-clamp oEPSP recordings. Whole-cell current-clamp recordings were performed as previously reported (Grueter and Winder, 2005; Grueter et al., 2006; Kash and Winder, 2006; Silberman et al., 2013). For current-clamp recordings, electrodes of 2.5–5.0 MΩ were filled with (in mM) as follows: 135 K^+-gluconate, 5 NaCl, 10 HEPES, 0.6 EGTA, 4 Na_2GTP (pH 7.2–7.4, osmolarity 290–295). There was no picrotoxin in the ACSF. After brain slice preparation, slices recovered for 1 h in a submerged holding chamber (25°C) containing oxygenated (95% O_2/5% CO_2) ACSF. After recovery in the holding chamber, slices were transferred to the recording chamber where they were continuously perfused with oxygenated and heated (25°C) ACSF at a rate of 2 ml/min. For optical whole-cell recordings, stimulation was produced from a Lamba XL light source shone through a bandpass filter. The blue light was guided from the light source through the objective lens using a double lamp-housing adapter, resulting in illumination of the slice. Light stimuli were ~2 ms in duration and occurred every 10 s. oEPSPs of 5–25 mV were recorded. After achieving whole-cell configuration, cells were allowed to equilibrate for a minimum of 5 min before baseline was started. Postsynaptic parameters were monitored continuously throughout the duration of the experiments. Data are represented as an average of the peak amplitude of 3 sweeps.

To determine type of current-clamp response, we first applied light stimulation to the slice before injecting any current into the cell to estab-

lish whether the cell was PBN-responsive. Approximately 1 of 10 cells was either PBN-unresponsive or the response generated by the light stimulation was too small to be appropriately interpreted and classified. The membrane potentials of the cells that we recorded from in the BNST rested between −70 mV and −85 mV before any current injection. Once it was determined that a BNST cell was PBN-responsive, we injected current into the cell until its membrane potential was between −45 mV and −60 mV. Within these membrane potentials, the cell would either fire or a feedforward IPSP would be generated. If the cell fired within these membrane potentials, we classified it as a PBN-excited cell; if an IPSP was observed, we classified the cell as a PBN-inhibited cell. For cell profile recordings, current was injected into cells until their membrane potential was between −50 mV and −60 mV. Progressive 10 pA current steps current were then delivered to the cell from which we determined input resistance. By visual inspection of the responses to hyperpolarizing current injection, we determined whether a cell exhibited I_h current. From the responses to depolarizing steps, we determined whether a cell demonstrated fast- or slow-rise action potentials. Fast-rise action potentials had an action potential rise time of ~25 ms, whereas slow-rise action potentials had a rise time of ~40 ms.

For drug application experiments, cell type was determined by injecting current until the cell membrane potential rested between −45 and −60 mV and then cell type was determined by visual inspection as described above. For PBN-inhibited cells, current was injected into the cell so that the IPSP was observed during drug-application recordings. A 5 min baseline of the IPSP was taken before drug application. For PBN-excited cells, no current was injected into the cell. A 5 min baseline of the EPSP observed at the resting membrane potential of the cell was taken before drug application.

All whole-cell data were recorded with Clampex version 10.2 and analyzed with pClamp version 10.2 (Molecular Devices). Recordings contained a 5 to 10 min baseline recording before drug application. All data points were normalized to the first 5 min of baseline. Plotted time courses for whole-cell experiments are represented as 30 s averages.

Statistics. Experiments comparing a difference to baseline were analyzed using a Student's *t* test. Experiments comparing baseline to two consecutive drug treatments were compared using a repeated-measures one-way ANOVA and a Tukey's multiple-comparisons test for pairwise comparisons of baseline versus guanfacine-treated, baseline versus atipamezole-treated, and guanfacine-treated versus atipamezole-treated. The significance of the presence of I_h currents in PBN-inhibited and PBN-excited cells were determined used a χ^2 test. χ^2 analysis was also used to determine whether the frequency of α_{2A}-AR-containing asymmetric axosomatic contacts was greater than those for symmetric axosomatic or asymmetric axodendritic contacts in both the dorsal and the ventral BNST. Results are reported in text and figure legends. Significant differences were defined as having a $p < 0.05$.

Reagents used. Guanfacine hydrochloride (Tocris Bioscience) stock solution was made in water. Picrotoxin (Tocris Bioscience) stock solution was made in DMSO. Atipamezole hydrochloride (Tocris Bioscience) stock solution was made in water. Kynurenic acid (Tocris Bioscience) was added directly to the ACSF. Primary antibodies included mouse monoclonal NeuN (Millipore Bioscience Research Reagents, MAB377; 1:1K), mouse monoclonal anti-GAD67 (Millipore, MAB5406; 1:800), and goat polyclonal anti-CGRP (Abcam, ab36001; 1:1K). Secondary antibodies labeled with Dylight 405 (715–475-150; 1:250) (for NeuN images), cy3 for GAD 67 (715–166-150; 1:1K, or cy5 (715–176-150; 1:1K) (for CGRP images) and raised in donkeys were purchased from Jackson ImmunoResearch Laboratories. For immunoelectron microscopy, the primary antibody mouse monoclonal anti-HA was used (Covance, clone 16B12; 1:500). The secondary antibody used was biotinylated horse anti-mouse IgG (Vector, BA2000; 1:200).

Results

PBN input to the dorsal anterior BNST elicits EPSCs that drive two classes of postsynaptic responses

We used an optogenetic strategy to activate PBN or BLA inputs to the BNST through stereotaxic injection of one of these regions with AAV5-CaMKIIα-ChR2:YFP (see Figs. 1*A*, *D2* and 4*F*, inset, right). After a minimum of 5 weeks, mice expressed ChR2-YFP at the injection site (Figs. 1*D2* and 4*F*, inset, right), as well as in axons within the BNST (Figs. 1 *D1* and 4*F*, inset, left).

In addition to visual inspection of the injection site, the specificity of the ChR2-YFP viral vector injection into the PBN was confirmed by fluorescent immunohistochemical colocalization of ChR2-YFP with CGRP, a high-fidelity marker of PBN inputs within the BNST (Shimada et al., 1985, 1989; Dobolyi et al., 2005). Axosomatic synapses containing CGRP are found in PBN projections to the dorsal BNST (Shimada et al., 1989; Dobolyi et al., 2005). CGRP-expressing neurons that project from the lateral PBN to the extended amygdala have been shown to have functional importance. For example, CGRP-containing neurons that project from the outer external lateral PBN to the central nucleus have been shown to modulate feeding behavior (Carter et al., 2013). Projections from the PBN to the BNST are also thought to be the only source of CGRP within the BNST (Shimada et al., 1985). Therefore, we used CGRP as a marker of PBN terminals in the BNST, although we cannot exclude the possibility that there may be other PBN inputs to the BNST that are not CGRP-containing. Colocalization of ChR2-YFP and anti-CGRP fluorescent label was seen in the dorsal BNST (Fig. 1*D1*), indicating that the PBN viral injections resulted in expression of ChR2-YFP in PBN axons in the dBNST. We also performed image analysis with ImageJ (Fiji) software to illustrate a colocalization of ChR2-YFP and CGRP in the BNST, further affirming that some CGRP-expressing PBN terminals in the BNST also express ChR2 (Fig. 1*C*). Additionally, as has previously been reported, CGRP immunoreactivity was densest in the dorsal anterolateral portions of the BNST (Fig. 1*F1*) (Dobolyi et al., 2005; Gungor and Pare, 2014). CGRP immunoreactivity was not observed in brains taken from CGRPα knock-out mouse brains (Fig. 1*F2*).

The PBN has previously been demonstrated to contain vGluT2-containing projection neurons (Niu et al., 2010; Kaur et al., 2013). We confirmed that CGRP immunoreactivity colocalized with vGluT2 in mouse BNST (Fig. 1*G*). Further, the pattern of ChR2-YFP that we observed in the BNST was overall similar to published CGRP immunoreactivity in the BNST (Dobolyi et al., 2005; Gungor and Pare, 2014). Therefore, we focused our recordings on the anterior dorsal lateral portions of the BNST. Using whole-cell patch-clamp recordings from dorsal anterolateral BNST neurons in acutely prepared brain slices, we confirmed that optical recruitment of these fibers in the BNST using full-field blue LED illumination produced EPSCs (optical EPSCs or oEPSCs). oEPSCs in BNST recorded from PBN-injected mice were observed in the vast majority of cells tested. We could see large oEPSCs ranging up to ~1 nA produced by full-field illumination. oEPSC sizes were reduced for study through the use of neutral density filters and manipulation of the aperture to produce amplitudes for analysis between 100 and 650 pA, therefore keeping all baseline oEPSCs within a defined amplitude range. We then stimulated the slice once every 10–20 s. One oEPSC was generated from each light stimulation. Evoked oEPSCs were of a very short, relatively invariant latency, consistent with monosynaptic excitation. Representative traces of the dual component oEPSC generated by stimulation of the PBN input to the BNST are shown in Figure 1*E*. The reversal potential of the synaptic inputs of the PBN onto BNST neurons was −2.7 mV. The AMPA/NMDA ratio of the PBN inputs to the BNST was 0.849 ± 0.122 ($n = 5$). Application of the AMPA receptor antagonist NBQX (10 μM) reduced the oEPSC at −70 mV (80.6 ± 6.1%, $t_{(2)} = 13.1$, $p < 0.01$, $n = 3$). Together, these data are consistent

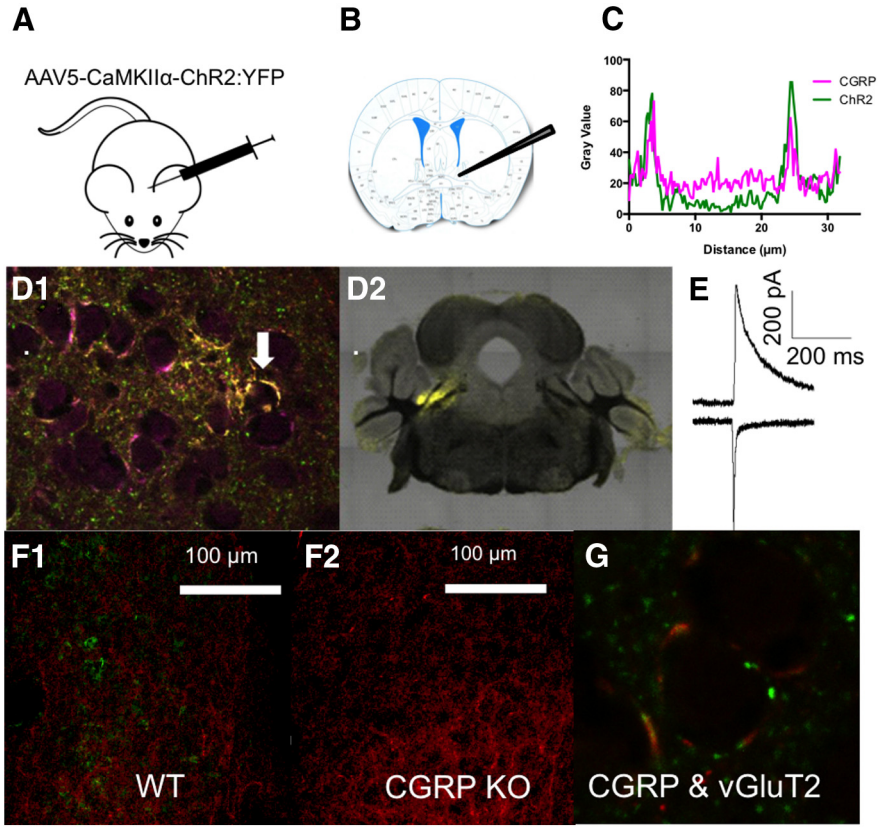

Figure 1. Optogenetic targeting of the parabrachial input to the BNST. ***A***, Illustrated mouse indicating that the experiments done in Figure 1***A–E*** used a C57BL/6J mouse that was injected with AAV5-CaMKIIα-ChR2:YFP at least 5 weeks prior. ***B***, Atlas image of BNST slice indicating that we are recording within the dorsal BNST while optically stimulating PBN terminals in the BNST (slice image adapted from the Franklin and Paxinos Mouse Brain Atlas). ***C***, Representative image of ImageJ (Fiji) image analysis done of a BNST cell and its surrounding neuropil after injection of AAV5-CaMKIIα-ChR2:YFP into the PBN of a C57BL/6J mouse 5 weeks prior. Colocalization of the gray value of CGRP (purple) with the gray value of ChR2 (green) is observed. ***D***, Image (63×) characterizing expression of ChR2-YFP in the BNST (***D1***, left) and at the PBN injection site (***D2***, right) 5 weeks after microinjection into the PBN. Left, Colocalization (yellow, indicated by white arrow) of CGRP (purple) with ChR2-YFP (green) in the dorsal BNST (***D1***). Right, ChR2-YFP expression (yellow) at the PBN injection site (***D2***). ***E***, Representative traces of the dual component oEPSC generated by stimulation of the PBN input to the BNST. ***F***, CGRP staining (green) can be seen in the dorsal anterolateral BNST of wild-type mice (***F1***, left) and is absent in CGRP KO mice (***F2***, right). GAD67 staining is shown in the dorsal BNST (red). ***G***, Colocalization of VGluT2 (green) with CGRP staining (red) in the dorsal anterolateral BNST.

with full-field illumination producing EPSCs from activation of the PBN projection to the BNST.

To establish the impact of the PBN input on BNST neuronal activity, we optically stimulated this input while recording in current-clamp mode. When activating PBN inputs to the BNST in *ex vivo* slices prepared from C57BL/6J mice that had been injected with AAV5-CaMKIIα-ChR2:YFP at least 5 weeks prior (Fig. 2*A*), we observed two overall types of responses to optical stimulation of the PBN input to the BNST. Some PBN afferents within the BNST end in large axosomatic terminal zones that envelop BNST neurons in a manner consistent with "detonator" type synapses, such as the climbing fiber input onto Purkinje neurons in cerebellum (Eccles et al., 1966; Shimada et al., 1989; Dobolyi et al., 2005). Thus, we predicted that we would observe PBN-induced firing in BNST neurons. In 18 of 34 neurons (52.7%) recorded from 14 mice, we indeed observed an EPSP followed by burst firing (Fig. 2*B1*,*B3*). In the remaining 16 neurons (41.7%), we observed a large IPSP in response to PBN stimulation (Fig. 2*B2*,*B3*). We hypothesized that this IPSP was generated by feedforward recruitment of GABA interneurons in the BNST, as recent evidence indicates a considerable amount of intra-BNST signaling (Poulin et al., 2009; Gungor and Pare, 2014). This was confirmed by blocking the IPSP through application of the ionotropic glutamate receptor antagonist kynurenic acid (4 mM; Fig. 2*D1*,*D2*,*E*) (89.9 ± 9.0%, $t_{(4)} = 10.0$, $p < 0.01$, $n = 5$).

Because the BNST contains many distinct cell types and we observed that two types of responses were exhibited by BNST neurons in response to stimulation of the PBN input, we examined the intrinsic excitable properties of these cells to determine whether the two types of responses were indicative of two populations of postsynaptic neurons. We injected hyperpolarizing and depolarizing current in a stepwise fashion through the patch-clamp electrode into both PBN-inhibited cells and PBN-excited cells in the BNST. We noted several features of the cells' responses to current injection that suggested commonality within these two response groups and distinctions across the groups (Fig. 2*C1–C3*). First, we saw that 56% ($n = 9$ of 16) of PBN-excited cells exhibited I_h current activity during hyperpolarizing steps, whereas only 20% ($n = 3$ of 15) of PBN-inhibited cells exhibited I_h current (Fig. 2*C1* compared with Fig. 2*C2*). χ^2 analysis of the presence of I_h current in each of the cell types revealed a significant difference between the PBN-inhibited and PBN-excited cells ($\chi^2 = 4.3$, df = 1, $p < 0.05$, $n = 31$). Second, PBN-excited cells had significant differences in their input resistances from PBN-inhibited cells, with the PBN-inhibited cells showing lower input resistances (371.0 MΩ ± 27.3 MΩ, $t_{(23)} = 3.1$, $p < 0.05$, $n = 13$) compared with higher input resistances in PBN-excited cells (494.1 MΩ ± 29.1 MΩ, $n = 12$). Third, we observed that PBN-inhibited cells had a slower rising phase on their action potentials (APs) based on visual inspection, with 15 of 16 PBN-inhibited cells showing slower rising APs, compared with PBN-excited cells where only 1 of 15 firing-type cells had slower rising APs (Fig. 2*C3*, slow-rise, bottom trace; compared with fast-rise, top trace). These differences between PBN-inhibited and PBN-excited cells indicate the possibility of two distinct populations of cells.

Ultrastructural analysis reveals widespread expression of α_{2A}-AR within the BNST and expression in asymmetric axosomatic synapses

α_{2A}-AR stimulation results in depression of excitatory drive in the BNST (Shields et al., 2009). Previous studies in the CeA suggest the possibility that α_2-ARs presynaptically regulate PBN input to that region (Delaney et al., 2007). To assess the localization of α_{2A}-ARs in the BNST, we used a genetically modified mouse in which an HA-tag was knocked-in to the N terminus of the α_{2A}-AR (Fig. 3*A1*). As antibodies for α_{2A}-ARs have poor specificity, we used this knock-in mouse so that we were able to visualize

α_{2A}-ARs using HA antibodies. Our previous light level localization of the α_{2A}-AR using this knock-in HA-tagged-α_{2A}-AR mouse line suggest heavy expression of this receptor postsynaptic to noradrenergic terminals, in that immunoreactivity far surpassed the pattern of TH staining (Shields et al., 2009). To more directly test the idea that α_{2A}-ARs are present on excitatory terminals in the BNST, we used immunoelectron microscopy to confirm a structural substrate for presynaptic action. We used the HA-α_{2A}-AR knock-in mice described above and used previously (Shields et al., 2009) (Fig. 3*A1*) and labeled BNST sections from these mice with an antibody directed against the HA tag.

Initially, we observed strong labeling when sections were examined with the light microscope; but when examined with the electron microscope, we observed only a few profiles containing DAB in the neuropil of the BNST. Instead, we observed what appeared to be DAB reaction product in the extracellular space outlining neuropil elements that themselves contained no clear label (Fig. 3*A2*). We reasoned that this was because the HA tag was attached to the N terminus of the receptor, a region predicted to be on the extracellular surface when the receptor is on the plasma membrane. Accordingly, we pretreated animals with the α_2-AR agonist clonidine before death to induce internalization of the receptor (Lu et al., 2009). We found that, with clonidine pretreatment, the extracellular label was greatly decreased and neuropil elements containing DAB label were more common. Dendritic shafts and preterminal axons appeared most commonly labeled in this clonidine-treated material, but dendritic spines and axon terminals could also be observed, as well as some glial processes (Fig. 3*B–E*). In some cases, the axon terminals could be observed making asymmetric synaptic contacts.

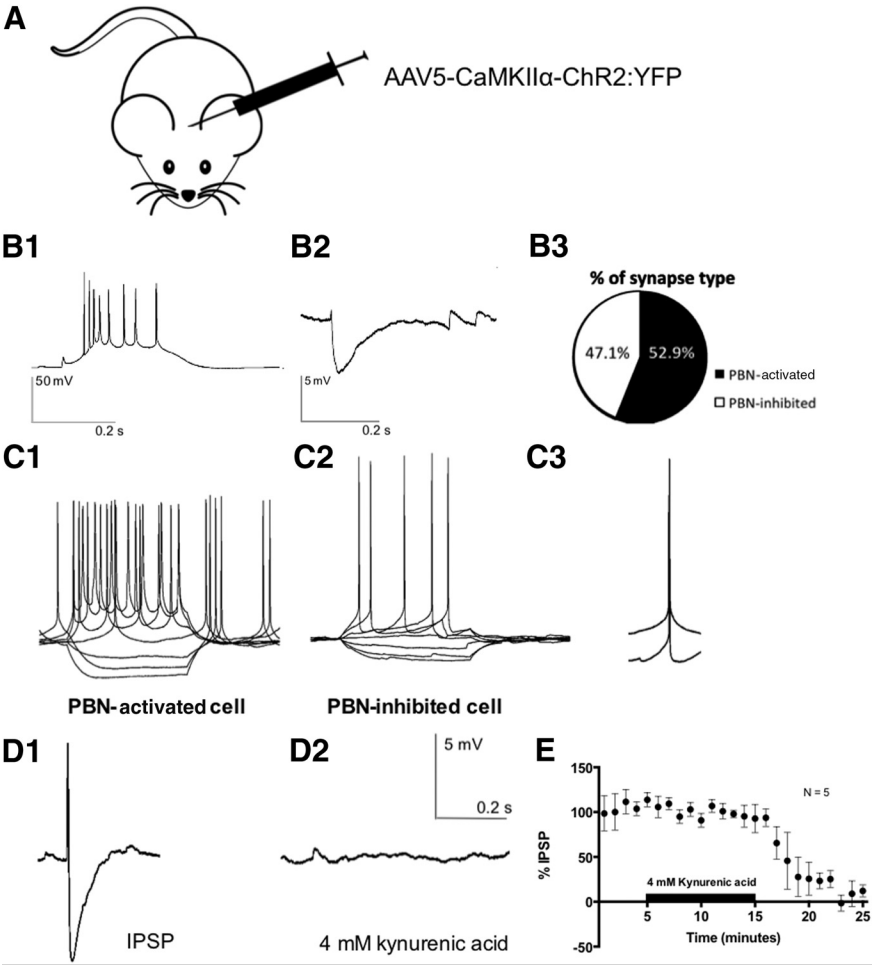

Figure 2. Parabrachial inputs to the BNST innervate at least two types of neurons. ***A***, Illustrated mouse indicating that the experiments done in Figure 2 used C57BL/6J mice that were injected with AAV5-CaMKIIα-ChR2:YFP at least 5 weeks prior. ***B***, A representative trace of a PBN-activated cell firing action potentials is shown (***B1***). A representative trace of an IPSP recorded from a PBN-inhibited cell is shown (***B2***). A pie chart showing the relative prevalence of each cell type is shown. PBN-activated cells comprise 52.9% of the 34 cells recorded from, and PBN-inhibited cells comprise 47.1% (***B3***). ***C***, Stepwise current injection into a PBN-activated cell; I_h current can be seen at hyperpolarized potentials (***C1***). Stepwise current injection into a PBN-inhibited cell; no I_h current is seen at hyperpolarized potentials (***C2***). Overlapping action potentials showing that action potentials generated in PBN-activated cells (top) have a faster rise time than PBN-inhibited cells (bottom) (***C3***). ***D***, Kynurenic acid (4 mM) blocks the feedforward IPSP generated by PBN-inhibited cells. Representative traces of an IPSP before drug application (***D1***) and after drug application (***D2***) are shown. ***E***, Time course showing the block of feedforward IPSPs generated in PBN-inhibited cells by kynurenic acid (4 mM) ($p < 0.01$, $n = 5$).

We were particularly interested in the labeled axon terminals. To determine the synaptology of α_{2A}-AR containing axon terminals in the dorsal BNST, we examined 235 images taken from the dorsal anterolateral BNST in four animals, representing 3872.5 μm^2. We identified a total of 106 asymmetric synapses in this sample: 40 terminated onto dendritic shafts and 66 onto dendritic spines. None of the axon terminals giving rise to asymmetric synapses onto dendritic shafts was labeled for α_{2A}-AR; 5% of the terminals synapsing onto dendritic spines were labeled for α_{2A}-AR (Fig. 3*F*).

Another possible target for α_{2A}-AR containing terminals in the BNST are cell bodies. Accordingly, we examined 34 cell bodies in dorsal anterolateral BNST. We identified all axon terminals making synaptic contacts onto these soma in the single ultrathin section. A total of 60 synaptic contacts were identified, 32 of which were asymmetric and 28 of which were symmetric. Of the terminals making symmetric contacts onto cell bodies, 7% contained label for α_{2A}-AR (Fig. 3*F*). On the other hand, 25% of the terminals making asymmetric synaptic contacts onto cell bodies were labeled for α_{2A}-AR (Fig. 3*F*).

We hypothesized that these α_{2A}-AR-containing terminals making axosomatic asymmetric synapses arose from parabrachial nucleus. To further evaluate this hypothesis, we examined the axon terminals in the ventral BNST. We reasoned that, if our hypothesis was correct, the percentage of labeled axosomatic synapses in the ventral BNST should be lower than in the dorsal BNST in keeping with the lighter parabrachial innervation of this region of the BNST. We examined 195 images taken from the ventral BNST in four animals, representing 3213.4 μm^2. We identified a total of 119 asymmetric synapses in this sample: 80 terminated onto dendritic shafts and 39 onto dendritic spines. Of the axon terminals giving rise to asymmetric synapses onto dendritic shafts, 11.3% were labeled for α_{2A}-AR; 7.7% of the

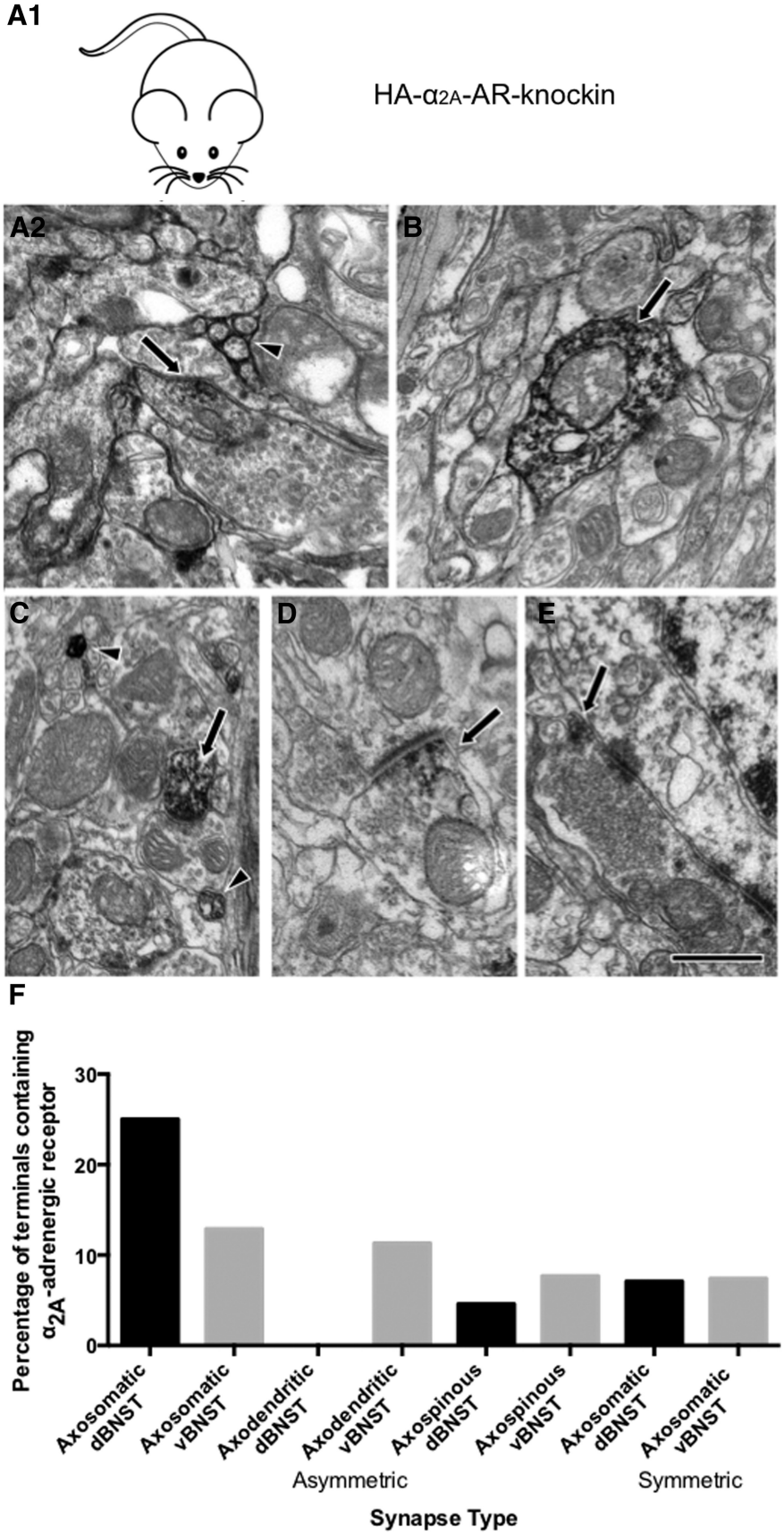

Figure 3. Immunolabeling for HA-tagged α_{2A}-AR in mouse BNST. ***A***, Illustrated mouse indicating that the experiments done in Figure 3 used HA-α_{2A}-AR-knockin mice (***A1***). Immunolabeling directed against the HA tag produced some patches of intracellular labeling in neuronal elements (arrow); however, the bulk of labeling observed appeared to be extracellular (arrowhead), appearing to fill spaces between elements of the neuropil, producing the effect of "outlining" them with reaction product (***A2***). ***B–E***, When animals were treated with clonidine before death, the "outlining" was less frequent and instead reaction product was observed inside neuronal elements. Dendrites (***B***, arrow) and preterminal axons (***C***, arrowheads) were commonly observed. Labeled dendritic spines (***C***, arrow) and axon terminals (***D***, ***E***, arrows) were also seen. The labeled axon terminals sometimes made asymmetric synaptic contacts (***E***). Scale bar, 500 nm. ***F***, Bar graph showing relative abundance of α_{2A}-ARs in each synapse type in both the dorsal and ventral BNST.

terminals synapsing onto dendritic spines were labeled for α_{2A}-AR. We then examined 43 cell bodies in ventral BNST. We identified all axon terminals making synaptic contacts onto these soma in the single ultrathin section. A total of 58 synaptic contacts were identified, 31 of which were asymmetric and 27 of which were symmetric. Of the terminals making symmetric contacts onto cell bodies, 7.4% contained label for α_{2A}-AR, whereas 12.9% of the terminals making asymmetric synaptic contacts onto cell bodies were labeled for α_{2A}-AR, approximately half the level seen for dorsal BNST (Fig. 3*F*). This is consistent with our hypothesis that these α_{2A}-AR containing axosomatic asymmetric synapses arise from the parabrachial nucleus.

We performed χ^2 analysis on our EM data for both the dorsal and ventral BNST to determine whether the frequency of α_{2A}-AR-containing contacts were greater in asymmetric axosomatic contacts versus symmetric axosomatic contacts. We also performed a χ^2 analysis to determine whether the frequency of α_{2A}-AR-containing contacts was greater in asymmetric axosomatic contacts versus asymmetric axodendritic contacts. In the dorsal BNST, there was no statistical difference in frequency of symmetric axosomatic α_{2A}-AR-containing contacts versus asymmetric axosomatic α_{2A}-AR-containing contacts ($\chi^2 = 3.4$, df $= 1$, not significant, $n = 60$). There was, however, a significant difference in the frequency of asymmetric axosomatic α_{2A}-AR-containing contacts compared with asymmetric axodendritic α_{2A}-AR-containing α_{2A}-ARs contacts ($\chi^2 = 11.3$, df $= 1$, $p < 0.01$, $n = 72$). In the ventral BNST, there was no significant difference between the frequency of asymmetric axosomatic α_{2A}-AR-containing contacts compared with either symmetric axosomatic α_{2A}-AR-containing contacts ($\chi^2 = 0.5$, df $=$ 1, not significant, $n = 58$) or to axodendritic

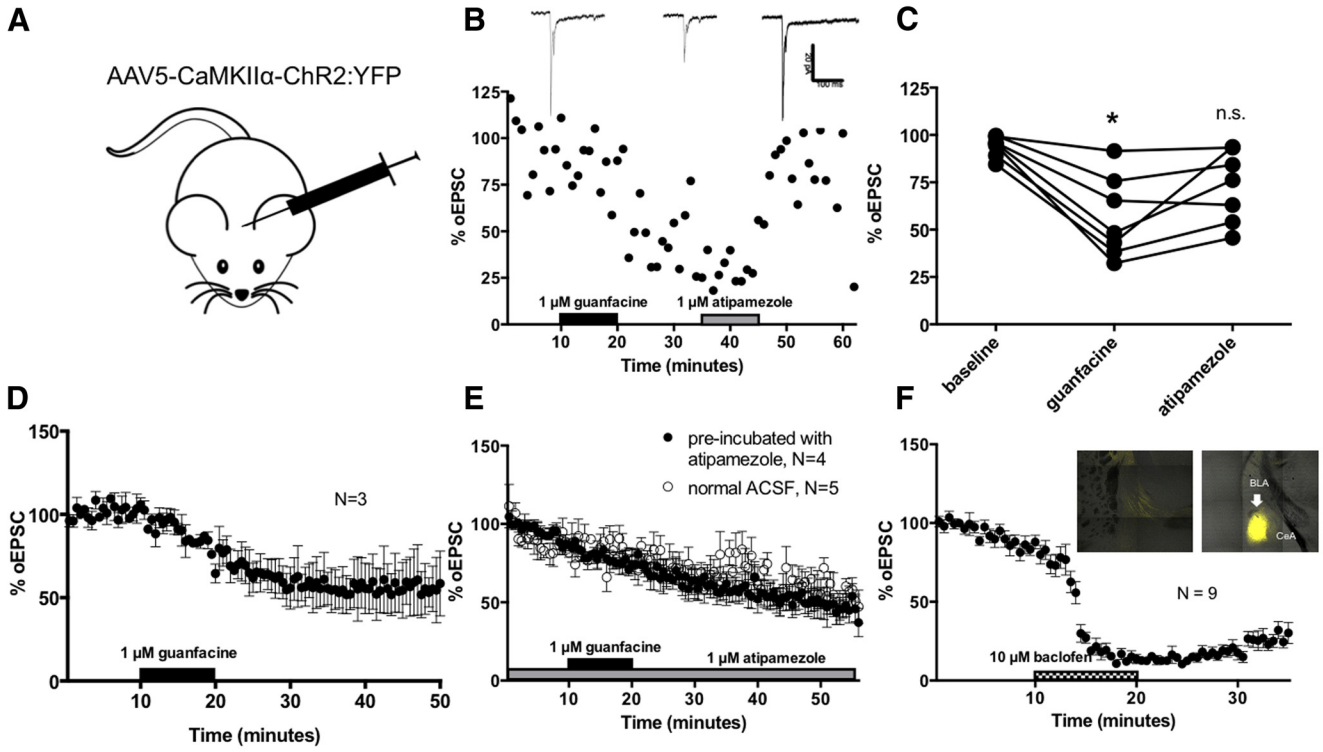

Figure 4. Guanfacine depresses excitatory transmission from the parabrachial nucleus projection to the BNST. ***A***, Illustrated mouse indicating that the experiments done in Figure 4 used C57BL/6J mice that were injected with AAV5-CaMKIIα-ChR2:YFP at least 5 weeks prior. ***B***, Individual experiment showing decrease in excitatory transmission of the PBN input to the BNST by guanfacine that is reversed by atipamezole (1 μM). Example traces of each phase of drug application are shown (insets). ***C***, Individual experiments showing that excitatory transmission is significantly decreased from baseline by guanfacine (1 μM) ($p < 0.01, n = 7$). Subsequent application of atipamezole reverses this depression such that amplitudes of oEPSCS are no longer significantly different from baseline (not significant, $n = 7$). *, Significant; n.s., not significant. ***D***, Guanfacine (1 μM) was applied to oEPSCs recorded from stimulation of the PBN afferents in the BNST. Guanfacine was allowed to washout for 30 min. With prolonged washout, the depression of the excitatory PBN input to the BNST did not reverse to baseline levels ($p < 0.05, n = 3$). ***E***, Guanfacine (1 μM) has no apparent effect on excitatory transmission from the BLA to the BNST in normal ACSF (white circles) ($p < 0.01, n = 5$). Preincubation of *ex vivo* BNST slices with atipamezole (1 μM) does not alter the effect of guanfacine on excitatory transmission from the BLA to the BNST (black circles) ($p < 0.01, n = 4$). ***F***, Baclofen (10 μM) depresses excitatory transmission from the BLA to the BNST ($p < 0.01, n = 9$). Image of the BLA injection site 5 weeks after injection of the AAV5-CaMKII α-ChR2:YFP into the BLA (inset, right). Expression of ChR2-YFP in the dorsal BNST 5 weeks after injection of the viral vector into the BLA (inset, left).

asymmetric α_{2A}-AR-containing contacts ($\chi^2 = 0.06$, df = 1, $n = 111$).

In total, these χ^2 analyses reveal that in the dorsal BNST there is a higher frequency of α_{2A}-AR-containing asymmetric axosomatic contacts than α_{2A}-AR-containing asymmetric axodendritic contacts. It also reveals that there is no significant difference between the α_{2A}-AR content of these types of synapses in the ventral BNST. This finding is consistent with what is known of the anatomy of the PBN input to the BNST, in which CGRP-containing axosomatic inputs from the PBN are predominantly observed in the dorsal BNST (Dobolyi et al., 2005). Although nonaxosomatic PBN inputs are observed in the ventral BNST, the overall density of PBN projections to the BNST are higher in the dorsal BNST than in the ventral BNST (Shimada et al., 1989; Alden et al., 1994). Therefore, the presence of α_{2A}-ARs on significantly more asymmetric axosomatic synapses selectively in the dorsal BNST is consistent with α_{2A}-AR expression on PBN terminals in this region.

Guanfacine suppresses oEPSCs elicited by PBN fiber recruitment in BNST

Given the likelihood that α_{2A}-ARs are present on PBN terminals in the BNST, we next assessed whether the α_{2A}-AR agonist guanfacine differentially affected individual inputs to the BNST using optogenetic strategies outlined in Figure 1. We tested the sensitivity of two different excitatory inputs to the BNST: the BLA and the PBN. We targeted the PBN input to the BNST as described above (Figs. 1 and 4*A*). Voltage-clamped whole-cell recordings were made in the presence of 25 μM picrotoxin to further isolate oEPSCs. Application of guanfacine (1 μM) depressed oEPSCs produced by activation of PBN afferents within the BNST (Fig. 4*B–D*) ($t_{(2,8)} = 9.4$, $p < 0.01$, $n = 7$). After application of the selective α_2 antagonist atipamezole (1 μM), the amplitude of oEPSCs returned to a level not significantly different from baseline (Fig. 4*B*,*C*). We did observe some variability across experiments (Fig. 4*C*). In some instances, such as the individual experiment (Fig. 4*B*), there was a clear depression of excitatory transmission by guanfacine that was reversed by atipamezole. In contrast, in other experiments, weaker effects of guanfacine on excitatory transmission were observed (Fig. 4*C*). Additionally, we performed experiments in which we applied guanfacine (1 μM) to oEPSCs recorded from stimulation of the PBN afferents in the BNST and then allowed for a long washout of guanfacine without subsequent application of atipamezole to the recordings (Fig. 4*D*). In such experiments, after prolonged washout of guanfacine, the size of oEPSC did not return to baseline levels (Fig. 4*D*) as was observed in Figure 4*B*, *C* (48.3 ± 11.2%, $t_{(2)} = 4.3$, $p < 0.05$, $n = 3$). Therefore, application of the α_2-AR antagonist ati-

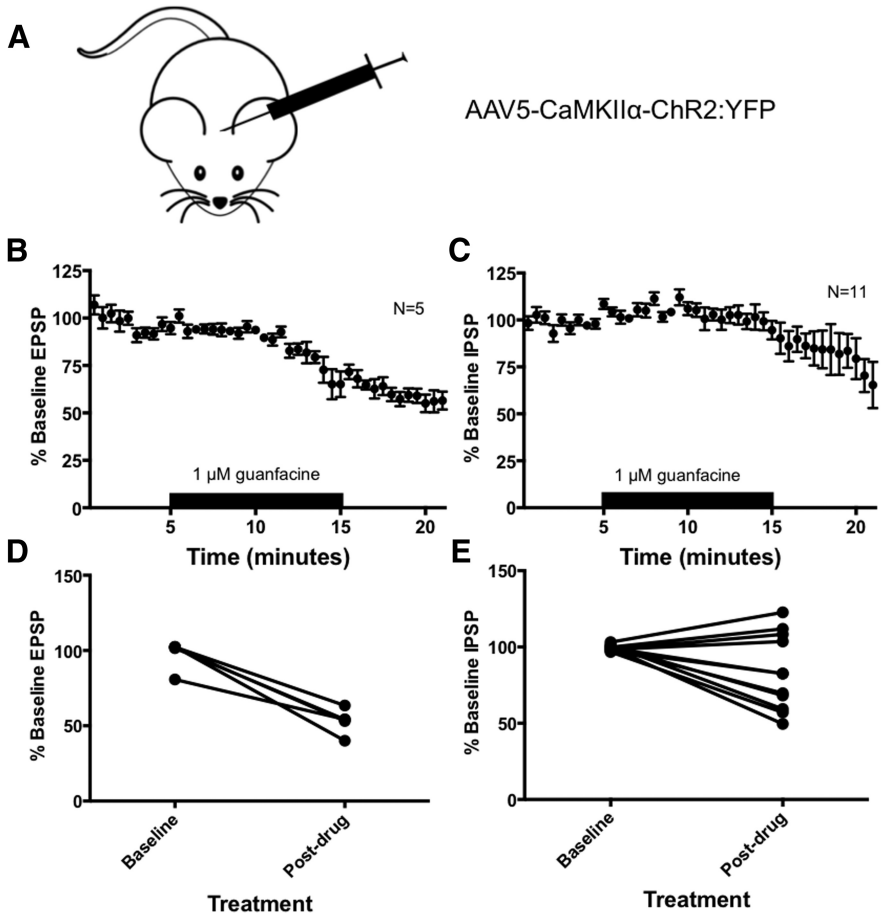

Figure 5. Guanfacine reduces EPSPs of PBN-activated cells in the BNST. ***A***, Illustrated mouse indicating that the experiments done in Figure 5 used C57BL/6J mice that were injected with AAV5-CaMKIIα-ChR2:YFP at least 5 weeks prior. ***B***, Guanfacine (1 μM) significantly decreases the size of EPSPs recorded from PBN-activated cells in the BNST ($p < 0.05$, $n = 5$). ***C***, Guanfacine (1 μM) has variable effects on IPSPs recorded from the PBN-inhibited cells in the BNST (not significant, $p = 11$). ***D***, Individual experiments showing the effect of guanfacine (1 μM) on EPSPs recorded from PBN-activated cells in the BNST. EPSPs are reduced by guanfacine across all experiments. ***E***, Individual experiments showing the effect of guanfacine (1 μM) on IPSPs recorded from PBN-activated cells in the BNST. The effect of guanfacine on IPSPs is more variable with IPSPs being reduced in some experiments and unaltered in others.

pamezole appears to be necessary for the reversal of the depression of excitatory transmission from the PBN to the BNST by guanfacine.

We also assessed the effect of guanfacine on oEPSCs produced by activation of BLA afferents within the BNST using a similar strategy involving injection of the ChR2-expressing viral vector (AAV5-CaMKIIα-ChR2:YFP) into the BLA 5–12 weeks before brain slice preparation. We observed expression of ChR2-YFP fluorescence at both the BLA injection site (Fig. 4*F*, inset, right) and in axons within the BNST (Fig. 4*F*, inset, left). Full-field illumination produced robust oEPSCs that were brought to a range of 100–650 pA through the use of neutral density filters and manipulations of the light aperture. The BLA input to the BNST, in the presence of picrotoxin, showed very little, if any, sensitivity to guanfacine (Fig. 4*E*, open circles) (32.4 ± 6.3%, $t_{(4)} = 5.2$, $p < 0.01$, $n = 5$). We observed marked rundown in the recordings of the BLA input to the BNST, but the extent of the rundown was the same when *ex vivo* BNST slices were preincubated in atipamezole (1 μM) (Fig. 4*E*, closed circles) (42.7 ± 6.2%, $t_{(3)} = 6.8$, $p < 0.01$, $n = 4$) or not (Fig. 4*E*, open circles). Because of the lack of difference between recordings done in normal ACSF and recordings done with atipamezole preincubation, we think that any differences in amplitude between oEPSCs recorded at baseline and oEPSCs recorded after guanfacine application were the result of rundown of recordings. In the case of these *ex vivo* optogenetic recordings, we refer to "rundown" as a decrease in the size of the oEPSC over the duration of the recording that appears to be independent of either a drug effect or of cell health. Interestingly, this rundown was observed in the BLA input to the BNST but not the PBN inputs. The 1 μM concentration of atipamezole used was previously sufficient to reverse the effect of α_{2A}-AR agonist actions on electrically evoked EPSCs (Shields et al., 2009). To ensure that we would be capable of observing $G_{i/o}$-protein coupled receptor modulation of BLA inputs in the BNST even with the rundown of the oEPSC, we examined actions of the $GABA_B$ agonist baclofen. The $GABA_B$ receptor is virtually ubiquitously expressed on glutamatergic terminals in the CNS, where it depresses glutamate release. Despite the rundown observed in our BLA-to-BNST recordings, we were able to observe robust depression of oEPSCs elicited by BLA fiber activation by baclofen (10 μM) (Fig. 4*F*) (69.6 ± 9.7%, $t_{(8)} = 7.2$, $p < 0.001$, $n = 9$). Although the level of expression of α_{2A}-ARs on BLA terminals in the BNST is unknown, our electrophysiological data suggest that excitatory transmission from the BLA input to the BNST is insensitive to activation of α_{2A}-ARs (Fig. 4*E*). These data suggest that guanfacine selectively modulates PBN inputs to the BNST.

Guanfacine depresses PBN-induced current-clamp responses on BNST neurons

As described above, we observed two types of membrane potential responses of BNST neurons to stimulation of the kPBN input: "PBN-excited" and "PBN-inhibited." We sought to determine whether there were any differences in the sensitivity of each type of response to guanfacine. We again targeted the PBN using the optogenetic strategies described above (Figs. 1 and 5*A*). For PBN-excited responses, we applied 1 μM guanfacine to the optically evoked EPSPs recorded from the BNST neuron at the cell's resting membrane potential. We observed that PBN-excited cells show a marked decrease in EPSP size with guanfacine application (Fig. 5*B*) (40.2 ± 6.0%, $t_{(4)} = 6.7$, $p < 0.01$, $n = 5$). Further, this decrease in EPSP size with guanfacine was seen in all PBN-excited cells that we tested (Fig. 5*D*). In contrast, although the PBN-inhibited cells showed a trend for a decrease in size of IPSP with 1 μM guanfacine application (Fig. 5*C*) (15.1 ± 7.4%, $t_{(10)} = 2.0$, not significant, $n = 11$), the decrease was not significant. Interestingly, we observed that some PBN-inhibited cells show a decrease in IPSP size with guanfacine application, whereas others did not (Fig. 5*E*). Therefore, the lack of significance of the

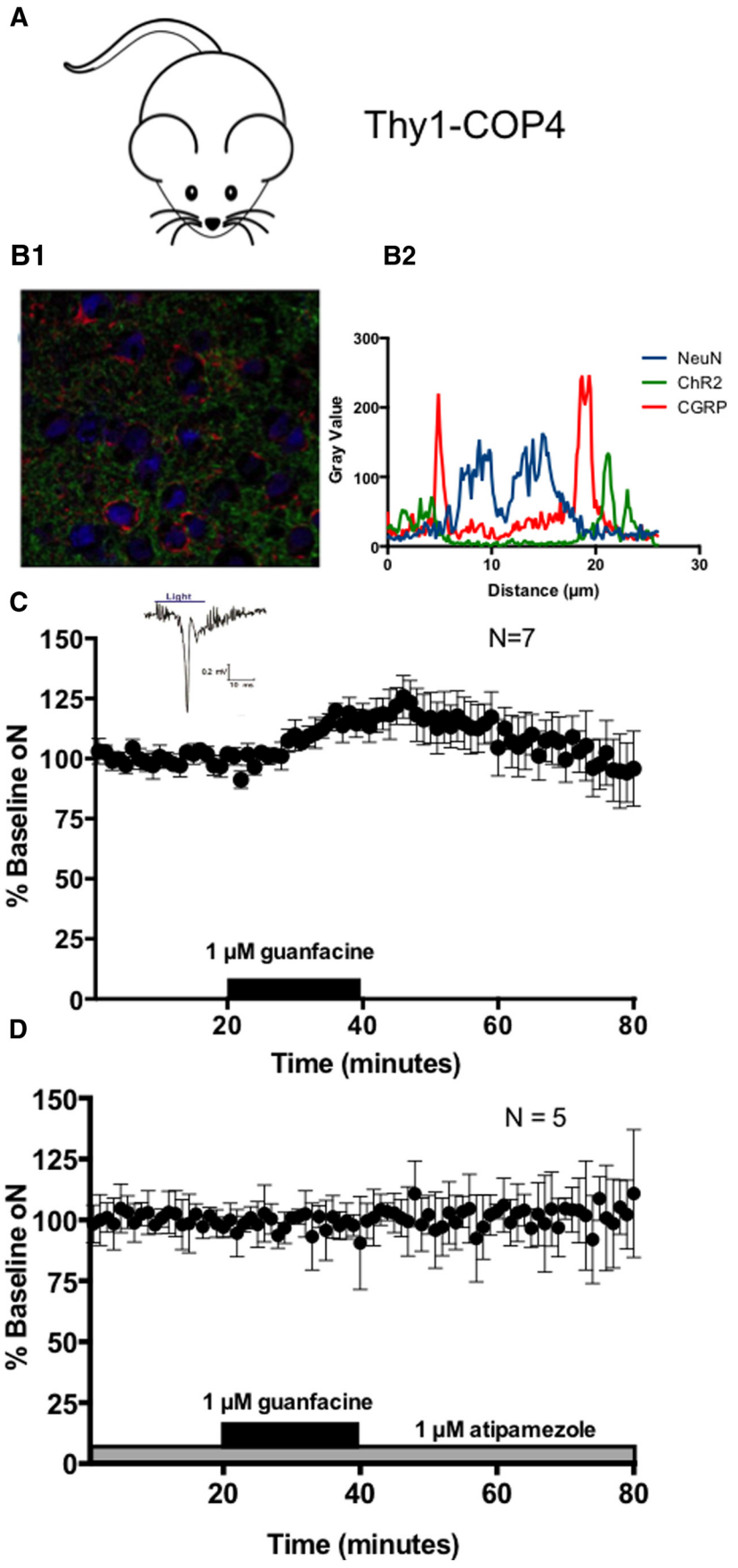

Figure 6. Guanfacine increases field potentials in the dBNST of Thy1-COP4 transgenic mice. ***A***, Illustrated mouse indicating that the experiments done in Figure 6 used Thy1-COP4 transgenic mice. ***B***, Image of dorsal BNST (63×) showing lack of colocalization of CGRP (red) with ChR2 (green) in Thy1-COP4 mice. NeuN staining is shown in blue (***B1***). Representative image of ImageJ (Fiji) analysis done of a BNST cell and its surrounding neuropil in a Thy1-COP4 transgenic mouse. ImageJ (Fiji) image analysis does not show colocalization of CGRP (red) with the ChR2 (green). There is also no observed colocalization of CGRP or ChR2 with NeuN (blue) (***B2***). ***C***, Optical field potential (oN) size is increased with guanfacine (1 μM) application in Thy1-COP4 mice ($p < 0.05$, $n = 7$). Representative trace of oN is shown (inset). ***D***, Preincubation of *ex vivo* BNST slices with atipamezole (1 μM) blocks the increase in size of the optical field potentials with subsequent guanfacine (1 μM) application (not significant, $n = 5$).

decrease in the IPSP may be the result of heterogeneity in the sensitivity to guanfacine of the PBN input onto each of these PBN-inhibited cells. Further, because these IPSPs are feedforward, the variability of the IPSPs response to guanfacine likely depends on the sensitivity of both the glutamatergic input and the intervening inhibitory interneuron to α_{2A}-AR activation by guanfacine.

Differential action of guanfacine on optically evoked excitatory responses in Thy1-COP4 mouse BNST

Analysis of extracellular field potentials can provide a more global analysis of the impact of modulatory receptors on circuit activity. In examining ChR2-YFP expression in Thy1-COP4 transgenic mice, we determined that, although ChR2-YFP was heavily expressed in regions that project to the BNST such as the BLA, cortical regions, and the hippocampus, ChR2-YFP did not colocalize with immunoreactivity from CGRP neuropeptide, a marker of a PBN input to the BNST (Fig. 6*A*,*B1*). We performed image analysis using ImageJ (Fiji) software to illustrate that the fluorescent signal from CGRP immunohistochemistry staining that surrounds dBNST cell bodies does not overlap with ChR2-YFP fluorescence in Thy1-COP4 mice. A representative image of this analysis is shown in Figure 6*B2*.

We prepared *ex vivo* slices from Thy1-COP4 transgenic mice and performed optical field potential recordings in the dBNST (Fig. 6*A*). We found that full-field optical stimulation in BNST slices from Thy1-COP4 mice produced a synchronized field potential response that was substantially reduced by AMPA receptor antagonists (76.2% from baseline, $n = 1$), which is consistent with N2 responses that we have previously published (Egli et al., 2005; Grueter and Winder, 2005). This indicates only a small amount of expression of ChR2 in postsynaptic BNST neurons in

this mouse line and that the optical field potential elicited is driven by recruitment of glutamatergic afferents. We found that we were able to elicit optical field potentials (oN) that were similar in size to our previously published N2 responses (Fig. 6*C*, inset) (Egli et al., 2005; Grueter and Winder, 2005).

Surprisingly, when we applied guanfacine (1 μM) to the optical extracellular field potential recordings, we observed an increase in the size of the oN (Fig. 6*C*) (18.6 ± 6.5%, $t_{(6)} = 2.9$, $p < 0.05$, $n = 7$). This increase in field potential size with guanfacine (1 μM) contrasts with our previous work done using electrical stimulation that shows a decrease in excitatory transmission with guanfacine application (Shields et al., 2009). This increase in optical field potential size with guanfacine application to *ex vivo* BNST slices of Thy1-COP4 mice was blocked by preincubation of slices with atipamezole (1 μM), further confirming this enhancement is mediated through activation of α_2-ARs (Fig. 6*D*) (0.1 ± 5.2%, $t_{(4)} = 0.02$, not significant, $n = 5$).

Discussion

Here we have optogenetically activated PBN inputs to the BNST for electrophysiological analysis. We find that full-field illumination of *ex vivo* BNST slices that have been prepared from mice with AAV5-CaMKIIα-ChR2:YFP injected into the PBN at least 5 weeks prior yields a dual component oEPSC that produces cell-type-specific responses. In one cell type, stimulation promotes robust feedforward inhibition. In another, stimulation produces repetitive firing. We found that the α_{2A}-AR agonist guanfacine filters excitatory drive into the BNST by depressing oEPSCs contributing to the depolarizing effects of the PBN input. Using immunoelectron microscopy and a novel knock-in HA-tagged α_{2A}-AR mouse strain, we show that α_{2A}-ARs are present on asymmetric axosomatic synapses in the dorsal BNST, which are consistent with localization to PBN inputs.

α_{2A}-ARs specifically modulate excitatory PBN inputs to the extended amygdala

In contrast to the PBN input to the BNST, our data suggest that the BLA input to the BNST is largely insensitive to guanfacine. These data are consistent with previous work examining the sensitivity of electrically evoked PBN and BLA inputs to the CeA (Delaney et al., 2007). Similar to our findings in the BNST, this work suggests that the PBN input to the CeA is depressed by α_2-ARs while the BLA is unaffected (Delaney et al., 2007). Although the relative expression of α_{2A}-ARs on the BLA terminals in the BNST is unknown, our study suggests that these terminals are insensitive to α_{2A}-AR activation.

Until the advent of optogenetic approaches, studies in which specific inputs to the BNST are targeted using electrical stimulation were not possible because of the close proximity of afferent fibers to the BNST. Through the use of *ex vivo* slice ChR2 recordings, we are now able to dissect neural circuits in ways that were previously not feasible by targeting individual inputs using optogenetic strategies outlined in this study. Here, we focus on the selective modulation of a PBN input to the dorsal BNST by α_{2A}-ARs because past behavioral work has shown that α_2-AR agonists in the dorsal BNST block stress-induced relapse to drug seeking behavior (Wang et al., 2001). However, recent work has shown that the PBN projects to the CeA and the vlBNST with differing densities (Bienkowski and Rinaman, 2013). In future work, it may be interesting to more closely study the impact of the PBN input to these regions on synaptic transmission. Here we demonstrate that optogenetic strategies can be used to explore neuromodulation of excitatory synapses from selective inputs to the BNST *ex vivo*.

α_2-ARs regulate axosomatic synapses in the extended amygdala and in the cerebellum

Our work in the context of other studies suggests similarity in PBN control of extended amygdala neurons and in climbing fiber control of Purkinje cells. First, the PBN input to the BNST shares anatomical features with the climbing fiber input in the cerebellum with heavy axosomatic innervation (Eccles et al., 1966; Shimada et al., 1989). Second, both generate two types of responses upon stimulation: pronounced firing or feedforward inhibition (Mathews et al., 2012). Third, both inputs are selectively regulated relative to other glutamate afferents in the respective regions by α_2-ARs (Carey and Regehr, 2009).

We observed that the PBN-initiated current-clamp responses in BNST have differential sensitivity to guanfacine. Both the multiple types of postsynaptic responses in the BNST to PBN stimulation and the variable sensitivity of these responses to guanfacine highlight the complex microcircuitry of the BNST. The BNST is composed of many cell types (Hammack et al., 2007); therefore, it is not surprising that these postsynaptic responses show variable sensitivity to guanfacine, in particular the feedforward PBN-inhibited responses where sensitivity of the intermediary interneuron to guanfacine is also a factor. Our data suggest that guanfacine administration may preferentially filter inhibition of one cell type over activation of another by the PBN. In future studies, determining the nature of these neurons, in particular whether they are projection neurons or interneurons, will begin to provide a more complete picture of how this circuit is regulated. Further, we cannot rule out the possibility of infection by our ChR2-expressing viral vector of CGRP-negative projections from the PBN to the BNST that could influence these responses in unforeseen ways.

Evidence for a possible excitatory role of α_{2A}-ARs in the BNST

To our surprise, we observed an increase in the size of an optically induced field potential by guanfacine in Thy1-COP4 mice. These mice have no observed colocalization of the neuropeptide CGRP, a marker of one PBN input to the BNST, with ChR2-YFP, and have very low postsynaptic expression of ChR2 in the BNST, suggesting that α_{2A}-ARs may enhance the actions of another excitatory input to the BNST. As shown in Figure 3, we do observe expression of the α_{2A}-ARs on other presynaptic terminal types. Another possibility is that postsynaptic α_{2A}-ARs in the BNST may increase the excitability of BNST cells. For example, postsynaptic α_{2A}-ARs can increase excitability by modulation of I_h, as has been shown in the prefrontal cortex (Wang et al., 2007). Furthermore, intraperitoneal injections of guanfacine increase c-fos expression in the BNST, suggesting a possible excitatory role for α_{2A}-ARs (Savchenko and Boughter, 2011), although other mechanisms could underlie the increase in c-fos expression with intraperitoneal injection of guanfacine. Finally, it is also possible that guanfacine is decreasing $GABA_B$ signaling or increasing glutamatergic signaling from another input.

The PBN input may influence downstream BNST signaling

Because of the behavioral effects of activation of α_{2A}-ARs in the BNST, it seems likely that the depression of the PBN input to the BNST by guanfacine that we observe here may alter downstream signaling of the BNST to brain regions involved in addiction and relapse, such as the VTA (Georges and Aston-Jones, 2001, 2002;

Dumont and Williams, 2004; Silberman et al., 2013) and the NAc (Dong et al., 2001). Alterations in the BNST's outputs may curb stress-induced drug cravings or stress-induced reemergence of negative symptoms of withdrawal. Indeed, it has been shown that guanfacine treatment reduces withdrawal-induced anxiety in rats treated with guanfacine (Buffalari et al., 2012). Additionally, it has been shown that injection of an α_2-AR agonist into the BNST will block withdrawal-induced place aversion (Delfs et al., 2000). Therefore, a decrease in excitatory transmission from the PBN to the BNST by α_{2A}-ARs may decrease the aversive withdrawal-like symptoms brought on by stress and help to prevent relapse.

In addition to stress-induced relapse to drug-seeking behaviors, the modulation of BNST signaling by the PBN input may influence anxiety-like behaviors and fear conditioning (Sink et al., 2011, 2013a, b; Gungor and Pare, 2014). The PBN input to other regions of the extended amygdala has been implicated in feeding behavior (Carter et al., 2013) and pain sensitization (Han et al., 2005; Han et al., 2010). The PBN efferents have also been implicated in taste aversion (Mungarndee et al., 2006) and hypercapnic arousal (Kaur et al., 2013). Therefore, the optogenetic strategies outlined in this study for the targeting of PBN inputs to the extended amygdala and other brain regions could be beneficial in better understanding a wide range of conditions, from anxiety disorders, to disorders of energy homeostasis, to pain disorders, to sleep apnea.

In conclusion, our work demonstrates divergent actions of the PBN input on cell responses in the BNST. We demonstrate that depolarizing effects of the PBN appear to be preferentially reduced by the α_{2A}-AR agonist guanfacine. Finally, we show that, in the relative absence of PBN signaling, guanfacine has very different actions on BNST excitability, suggesting a state-dependent aspect to the actions of guanfacine. In future work, it will be important to examine the consequences of specific regulation of the PBN *in vivo* by guanfacine.

References

Alden M, Besson JM, Bernard JF (1994) Organization of the efferent projections from the pontine parabrachial area to the bed nucleus of the stria terminalis and neighboring regions: a PHA-L study in the rat. J Comp Neurol 341:289–314. CrossRef Medline

Arenkiel BR, Peca J, Davison IG, Feliciano C, Deisseroth K, Augustine GJ, Ehlers MD, Feng G (2007) In vivo light-induced activation of neural circuitry in transgenic mice expressing channelrhodopsin-2. Neuron 54: 205–218. CrossRef Medline

Aston-Jones G, Delfs JM, Druhan J, Zhu Y (1999) The bed nucleus of the stria terminalis: a target site for noradrenergic actions in opiate withdrawal. Ann N Y Acad Sci 877:486–498. CrossRef Medline

Bienkowski MS, Rinaman L (2013) Common and distinct neural inputs to the medial central nucleus of the amygdala and anterior ventrolateral bed nucleus of stria terminalis in rats. Brain Struct Funct 218:187–208. CrossRef Medline

Brown SA, Vik PW, Patterson TL, Grant I, Schuckit MA (1995) Stress, vulnerability and adult alcohol relapse. J Stud Alcohol 56:538–545. Medline

Buffalari DM, Baldwin CK, See RE (2012) Treatment of cocaine withdrawal anxiety with guanfacine: relationships to cocaine intake and reinstatement of cocaine seeking in rats. Psychopharmacology 223:179–190. CrossRef Medline

Carey MR, Regehr WG (2009) Noradrenergic control of associative synaptic plasticity by selective modulation of instructive signals. Neuron 62: 112–122. CrossRef Medline

Carter ME, Soden ME, Zweifel LS, Palmiter RD (2013) Genetic identification of a neural circuit that suppresses appetite. Nature 503:111–114. CrossRef Medline

Delaney AJ, Crane JW, Sah P (2007) Noradrenaline modulates transmission at a central synapse by a presynaptic mechanism. Neuron 56:880–892. CrossRef Medline

Delfs JM, Zhu Y, Druhan JP, Aston-Jones G (2000) Noradrenaline in the ventral forebrain is critical for opiate withdrawal-induced aversion. Nature 403:430–434. CrossRef Medline

Dobolyi A, Irwin S, Makara G, Usdin TB, Palkovits M (2005) Calcitonin gene-related peptide-containing pathways in the rat forebrain. J Comp Neurol 489:92–119. CrossRef Medline

Dong HW, Petrovich GD, Watts AG, Swanson LW (2001) Basic organization of projections from the oval and fusiform nuclei of the bed nuclei of the stria terminalis in adult rat brain. J Comp Neurol 436:430–455. CrossRef Medline

Dumont EC, Williams JT (2004) Noradrenaline triggers GABAA inhibition of bed nucleus of the stria terminalis neurons projecting to the ventral tegmental area. J Neurosci 24:8198–8204. CrossRef Medline

Eccles JC, Llinás R, Sasaki K (1966) The excitatory synaptic action of climbing fibres on the Purkinje cells of the cerebellum. J Physiol 182:268–296. Medline

Egli RE, Kash TL, Choo K, Savchenko V, Matthews RT, Blakely RD, Winder DG (2005) Norepinephrine modulates glutamatergic transmission in the bed nucleus of the stria terminalis. Neuropsychopharmacology 30: 657–668. CrossRef Medline

Erb S, Hitchcott PK, Rajabi H, Mueller D, Shaham Y, Stewart J (2000) Alpha-2 adrenergic receptor agonists block stress-induced reinstatement of cocaine seeking. Neuropsychopharmacology 23:138–150. CrossRef Medline

Erb S, Shaham Y, Stewart J (2001) Stress-induced relapse to drug seeking in the rat: role of the bed nucleus of the stria terminalis and amygdala. Stress 4:289–303. CrossRef Medline

Flavin SA, Winder DG (2013) Noradrenergic control of the bed nucleus of the stria terminalis in stress and reward. Neuropharmacology 70:324–330. CrossRef Medline

Fox H, Sinha R (2014) The role of guanfacine as a therapeutic agent to address stress-related pathophysiology in cocaine-dependent individuals. Adv Pharmacol 69:217–265. CrossRef Medline

Fox HC, Morgan PT, Sinha R (2014) Sex differences in guanfacine effects on drug craving and stress arousal in cocaine-dependent individuals. Neuropsychopharmacology 39:1527–1537. CrossRef Medline

Georges F, Aston-Jones G (2001) Potent regulation of midbrain dopamine neurons by the bed nucleus of the stria terminalis. J Neurosci 21:RC160. Medline

Georges F, Aston-Jones G (2002) Activation of ventral tegmental area cells by the bed nucleus of the stria terminalis: a novel excitatory amino acid input to midbrain dopamine neurons. J Neurosci 22:5173–5187. Medline

Grueter BA, Winder DG (2005) Group II and III metabotropic glutamate receptors suppress excitatory synaptic transmission in the dorsolateral bed nucleus of the stria terminalis. Neuropsychopharmacology 30:1302–1311. CrossRef Medline

Grueter BA, Gosnell HB, Olsen CM, Schramm-Sapyta NL, Nekrasova T, Landreth GE, Winder DG (2006) Extracellular-signal regulated kinase 1-dependent metabotropic glutamate receptor 5-induced long-term depression in the bed nucleus of the stria terminalis is disrupted by cocaine administration. J Neurosci 26:3210–3219. CrossRef Medline

Gungor NZ, Pare D (2014) CGRP inhibits neurons of the bed nucleus of the stria terminalis: implications for the regulation of fear and anxiety. J Neurosci 34:60–65. CrossRef Medline

Hammack SE, Mania I, Rainnie DG (2007) Differential expression of intrinsic membrane currents in defined cell types of the anterolateral bed nucleus of the stria terminalis. J Neurophysiol 98:638–656. CrossRef Medline

Han JS, Li W, Neugebauer V (2005) Critical role of calcitonin gene-related peptide 1 receptors in the amygdala in synaptic plasticity and pain behavior. J Neurosci 25:10717–10728. CrossRef Medline

Han JS, Adwanikar H, Li Z, Ji G, Neugebauer V (2010) Facilitation of synaptic transmission and pain responses by CGRP in the amygdala of normal rats. Mol Pain 6:10. CrossRef Medline

Highfield D, Yap J, Grimm JW, Shalev U, Shaham Y (2001) Repeated lofexidine treatment attenuates stress-induced, but not drug cues-induced reinstatement of a heroin-cocaine mixture (speedball) seeking in rats. Neuropsychopharmacology 25:320–331. CrossRef Medline

Jobes ML, Ghitza UE, Epstein DH, Phillips KA, Heishman SJ, Preston KL (2011) Clonidine blocks stress-induced craving in cocaine users. Psychopharmacology 218:83–88. CrossRef Medline

Kash TL, Winder DG (2006) Neuropeptide Y and corticotropin-releasing factor bi-directionally modulate inhibitory synaptic transmission in the

bed nucleus of the stria terminalis. Neuropharmacology 51:1013–1022. CrossRef Medline

Kaur S, Pedersen NP, Yokota S, Hur EE, Fuller PM, Lazarus M, Chamberlin NL, Saper CB (2013) Glutamatergic signaling from the parabrachial nucleus plays a critical role in hypercapnic arousal. J Neurosci 33:7627–7640. CrossRef Medline

Krawczyk M, Georges F, Sharma R, Mason X, Berthet A, Bézard E, Dumont EC (2011) Double-dissociation of the catecholaminergic modulation of synaptic transmission in the oval bed nucleus of the stria terminalis. J Neurophysiol 105:145–153. CrossRef Medline

Lee A, Rosin DL, Van Bockstaele EJ (1998) alpha2A-adrenergic receptors in the rat nucleus locus coeruleus: subcellular localization in catecholaminergic dendrites, astrocytes, and presynaptic axon terminals. Brain Res 795:157–169. CrossRef Medline

Lu R, Li Y, Zhang Y, Chen Y, Shields AD, Winder DG, Angelotti T, Jiao K, Limbird LE, Zhou Y, Wang Q (2009) Epitope-tagged receptor knock-in mice reveal that differential desensitization of alpha2-adrenergic responses is because of ligand-selective internalization. J Biol Chem 284: 13233–13243. CrossRef Medline

Mantsch JR, Weyer A, Vranjkovic O, Beyer CE, Baker DA, Caretta H (2010) Involvement of noradrenergic neurotransmission in the stress- but not cocaine-induced reinstatement of extinguished cocaine-induced conditioned place preference in mice: role for beta-2 adrenergic receptors. Neuropsychopharmacology 35:2165–2178. CrossRef Medline

Mathews PJ, Lee KH, Peng Z, Houser CR, Otis TS (2012) Effects of climbing fiber driven inhibition on Purkinje neuron spiking. J Neurosci 32:17988–17997. CrossRef Medline

McElligott ZA, Winder DG (2008) Alpha1-adrenergic receptor-induced heterosynaptic long-term depression in the bed nucleus of the stria terminalis is disrupted in mouse models of affective disorders. Neuropsychopharmacology 33:2313–2323. CrossRef Medline

Milner TA, Lee A, Aicher SA, Rosin DL (1998) Hippocampal alpha2a-adrenergic receptors are located predominantly presynaptically but are also found postsynaptically and in selective astrocytes. J Comp Neurol 395:310–327. CrossRef Medline

Milner TA, Rosin DL, Lee A, Aicher SA (1999) Alpha2A-adrenergic receptors are primarily presynaptic heteroreceptors in the C1 area of the rat rostral ventrolateral medulla. Brain Res 821:200–211. CrossRef Medline

Muly EC, Maddox M, Smith Y (2003) Distribution of mGluR1alpha and mGluR5 immunolabeling in primate prefrontal cortex. J Comp Neurol 467:521–535. CrossRef Medline

Mungarndee SS, Lundy RF Jr, Norgren R (2006) Central gustatory lesions and learned taste aversions: unconditioned stimuli. Physiol Behav 87: 542–551. CrossRef Medline

Niu JG, Yokota S, Tsumori T, Qin Y, Yasui Y (2010) Glutamatergic lateral parabrachial neurons innervate orexin-containing hypothalamic neurons in the rat. Brain Res 1358:110–122. CrossRef Medline

Paxinos G, Franklin KB (2004) The mouse brain in stereotaxic coordinates. San Diego: Elsevier.

Poulin JF, Arbour D, Laforest S, Drolet G (2009) Neuroanatomical characterization of endogenous opioids in the bed nucleus of the stria terminalis. Prog Neuropsychopharmacol Biol Psychiatry 33:1356–1365. CrossRef Medline

Savchenko VL, Boughter JD Jr (2011) Regulation of neuronal activation by Alpha2A adrenergic receptor agonist. Neurotox Res 20:226–239. CrossRef Medline

Shaham Y, Highfield D, Delfs J, Leung S, Stewart J (2000) Clonidine blocks stress-induced reinstatement of heroin seeking in rats: an effect independent of locus coeruleus noradrenergic neurons. Eur J Neurosci 12:292–302. CrossRef Medline

Shields AD, Wang Q, Winder DG (2009) alpha2A-adrenergic receptors heterosynaptically regulate glutamatergic transmission in the bed nucleus of the stria terminalis. Neuroscience 163:339–351. CrossRef Medline

Shimada S, Shiosaka S, Emson PC, Hillyard CJ, Girgis S, MacIntyre I, Tohyama M (1985) Calcitonin gene-related peptidergic projection from the parabrachial area to the forebrain and diencephalon in the rat: an immunohistochemical analysis. Neuroscience 16:607–616. CrossRef Medline

Shimada S, Inagaki S, Kubota Y, Kito S, Funaki H, Takagi H (1989) Light and electron microscopic studies of calcitonin gene-related peptide-like immunoreactive terminals in the central nucleus of the amygdala and the bed nucleus of the stria terminalis of the rat. Exp Brain Res 77:217–220. Medline

Silberman Y, Matthews RT, Winder DG (2013) A corticotropin releasing factor pathway for ethanol regulation of the ventral tegmental area in the bed nucleus of the stria terminalis. J Neurosci 33:950–960. CrossRef Medline

Sinha R, Catapano D, O'Malley S (1999) Stress-induced craving and stress response in cocaine dependent individuals. Psychopharmacology 142: 343–351. CrossRef Medline

Sinha R, Kimmerling A, Doebrick C, Kosten TR (2007) Effects of lofexidine on stress-induced and cue-induced opioid craving and opioid abstinence rates: preliminary findings. Psychopharmacology 190:569–574. CrossRef Medline

Sinha R, Shaham Y, Heilig M (2011) Translational and reverse translational research on the role of stress in drug craving and relapse. Psychopharmacology 218:69–82. CrossRef Medline

Sink KS, Walker DL, Yang Y, Davis M (2011) Calcitonin gene-related peptide in the bed nucleus of the stria terminalis produces an anxiety-like pattern of behavior and increases neural activation in anxiety-related structures. J Neurosci 31:1802–1810. CrossRef Medline

Sink KS, Davis M, Walker DL (2013a) CGRP antagonist infused into the bed nucleus of the stria terminalis impairs the acquisition and expression of context but not discretely cued fear. Learn Mem 20:730–739. CrossRef Medline

Sink KS, Chung A, Ressler KJ, Davis M, Walker DL (2013b) Anxiogenic effects of CGRP within the BNST may be mediated by CRF acting at BNST CRFR1 receptors. Behav Brain Res 243:286–293. CrossRef Medline

Wang M, Ramos BP, Paspalas CD, Shu Y, Simen A, Duque A, Vijayraghavan S, Brennan A, Dudley A, Nou E, Mazer JA, McCormick DA, Arnsten AF (2007) Alpha2A-adrenoceptors strengthen working memory networks by inhibiting cAMP-HCN channel signaling in prefrontal cortex. Cell 129:397–410. CrossRef Medline

Wang X, Cen X, Lu L (2001) Noradrenaline in the bed nucleus of the stria terminalis is critical for stress-induced reactivation of morphine-conditioned place preference in rats. Eur J Pharmacol 432:153–161. CrossRef Medline

Weiss F, Koob GF (2001) Drug addiction: functional neurotoxicity of the brain reward systems. Neurotox Res 3:145–156. CrossRef Medline

Weitlauf C, Egli RE, Grueter BA, Winder DG (2004) High-frequency stimulation induces ethanol-sensitive long-term potentiation at glutamatergic synapses in the dorsolateral bed nucleus of the stria terminalis. J Neurosci 24:5741–5747. CrossRef Medline